Advanced Steel Construction – Vol. 18 No. 2 (2022) 536–543
DOI:10.18057/IJASC.2022.18.2.2

EXPERIMENTAL STUDY ON FATIGUE PERFORMANCE OF STEEL-CONCRETE JOINT SECTION OF HYBRID GIRDER CABLE-STAYED BRIDGE

Yang Zhou [1, *], Qian-Hui Pu [2], Zhou Shi [2], Hong-Ye Gou [2] and Shi-Li Yang [2]

[1] *School of Architecture and Civil Engineering, Chengdu University, Chengdu, 610106, P.R. China*
[2] *Key Laboratory of Transportation Tunnel Engineering, Ministry of Education, School of Civil Engineering, Southwest Jiaotong University, Chengdu, 610031, P.R. China*
** (Corresponding author: E-mail: zhouyangswjtu@163.com)*

ABSTRACT

In this paper, a localized full-scale model of a steel-concrete joint section of a hybrid girder cable-stayed bridge is designed and fabricated based on the stress equivalent principle and Miner's rule for cumulative linear damage caused by fatigue. The fatigue performance of this joint section is studied through both fatigue verification and failure loading, and the stresses of various structural members of the section are tested during loading processes. The results show that the stress values at various test points of the steel structure and shear connectors remain basically unchanged during a fatigue verification test of 2 million load cycles. After a fatigue test of 3 million load cycles, the stress level of the bottom and web plates on the steel structure increases slightly, the shear studs with larger stresses near the loading end enter a plastic state, and the overall rigidity decreases. Moreover, although the stress level of perforated-bonding (PBL) shear connectors increases gradually, the linear stress state is maintained. The load-carrying ratio of the shear studs decreases, while that of the PBL shear connectors rises. The stresses at the test points of the concrete structure are essentially unchanged before and after the fatigue tests, and the fatigue load has little effect on the stress of the concrete structure. The design of the joint section is reasonable and may be referenced for similar future projects.

ARTICLE HISTORY

Received: 5 August 2020
Revised: 11 August 2021
Accepted: 11 August 2021

KEYWORDS

Hybrid girder cable-stayed bridge;
Steel-concrete joint section;
Fatigue model test;
Fatigue performance

1. Introduction

Over the past few decades, many bridges with composite structures have emerged to improve the carrying and spanning capacities of bridges[1-4]. One example is the hybrid girder bridge, which uses steel and concrete girders for its main and side spans, respectively. Due to its superior carrying and spanning capacities, this design is widely applied to large-span bridges, especially large-span cable-stayed bridges. At present, hybrid girder cable-stayed bridges are mainly used for highway bridges, such as the Tatara Bridge (Japan), the Normandy Bridge (France), and the Stonecutters Bridge (China), and seldom used for railways. As speed, load, and span requirements for high-speed railways continually increase, hybrid cable-stayed bridges are gradually being utilized for railway bridges[5].

The steel-concrete joint section is the connecting part of the steel girder and concrete girder. It is usually comprised of a bearing plate, steel cells, shear connectors, prestressed steel bars and a concrete girder [6, 7]. Scholars have conducted extensive research on its design rationality and carrying capacity[8, 9]. For example, a Japanese scholar carried out a total cross-section model test with a similitude ratio of 1:50 and a half-section model test with a similitude ratio of 1:200 on the steel-concrete joint section of the Tatara Bridge. Zhang et al.[10] conducted a model test with a contracting ratio of 1:2 on the steel-concrete joint section of the Hero Bridge in Nanchang, in which the normal stress distribution and the bearing capacity of the joint section were studied by applying static force loading on the test model. The complex structures of the joint section experienced fatigue loading under long-term repeated vehicle loads[11-17]. However, there are few reports on the fatigue performance of steel-concrete joint sections. Furthermore, the fatigue problem is more prominent in the joint section of railway bridges because the proportion of live vehicle loads for railway bridges is larger than that of highway bridges and the greater bridge vibration caused by trains. Therefore, it is necessary to study and analyse the fatigue performance of steel-concrete joint sections for railway bridges[13-15]. Due to the complex design, it is difficult to accurately simulate the interactions and fatigue performances among the various structural members of the joint section by using the finite element method[18-20]. Meanwhile, due to the limitation of the test site and loading equipment, studies on static characteristics of joint sections have often been carried out through reduced-scale model tests based on similarity theory and Saint-Venant's Principle; however, such scale models cannot truly reflect initial structural imperfections and residual stresses. Thus, a study on the fatigue performance of the joint section is required based on full-scale model tests [21-23] .

In this paper, the fatigue performance of the steel-concrete joint section for the Yong-Jiang Bridge is discussed. The Yong-Jiang Bridge is a railway hybrid girder cable-stayed bridge located in Ningbo Zhejiang, China. The Yong-Jiang Bridge has a main span of 468 m, and a steel-concrete joint section is 7.35 m long, which is located at the main girder near the pylon and in a structure with a bearing plate and steel cells. The top plate of the joint section has 27 cells, and the bottom plate has 24 cells. The top and bottom plates in each steel cell are 28 mm thick, and the longitudinal diaphragm plate is 16 mm thick. The top and bottom plates feature Φ22-mm shear studs to enhance the bonding between the steel box girder and the concrete girder. Inside the joint section, there are two diaphragm plates spaced 1366 mm apart. The web plate features Φ60-mm holes, through which Φ25-mm reinforcing steel bars are inserted to form perforated-bonding (PBL) shear connectors. The web plate is connected to the concrete girder through the PBL shear connectors. In addition, a 60-mm thick steel plate is positioned between the steel girder and the concrete girder to serve as the bearing plate. The longitudinal prestressing force locks the plate to the concrete girder. A cross-sectional view and an elevation view of the steel-concrete section are shown (Figs. 1-2).

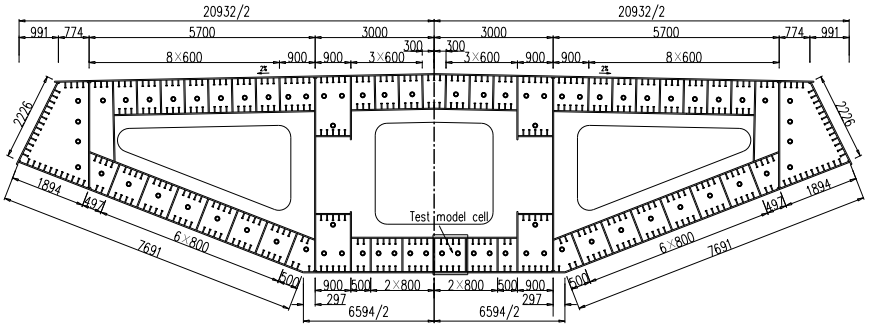

Fig. 1 Cross-sectional view of the steel-concrete joint section in the Yong-Jiang Bridge (unit: mm)

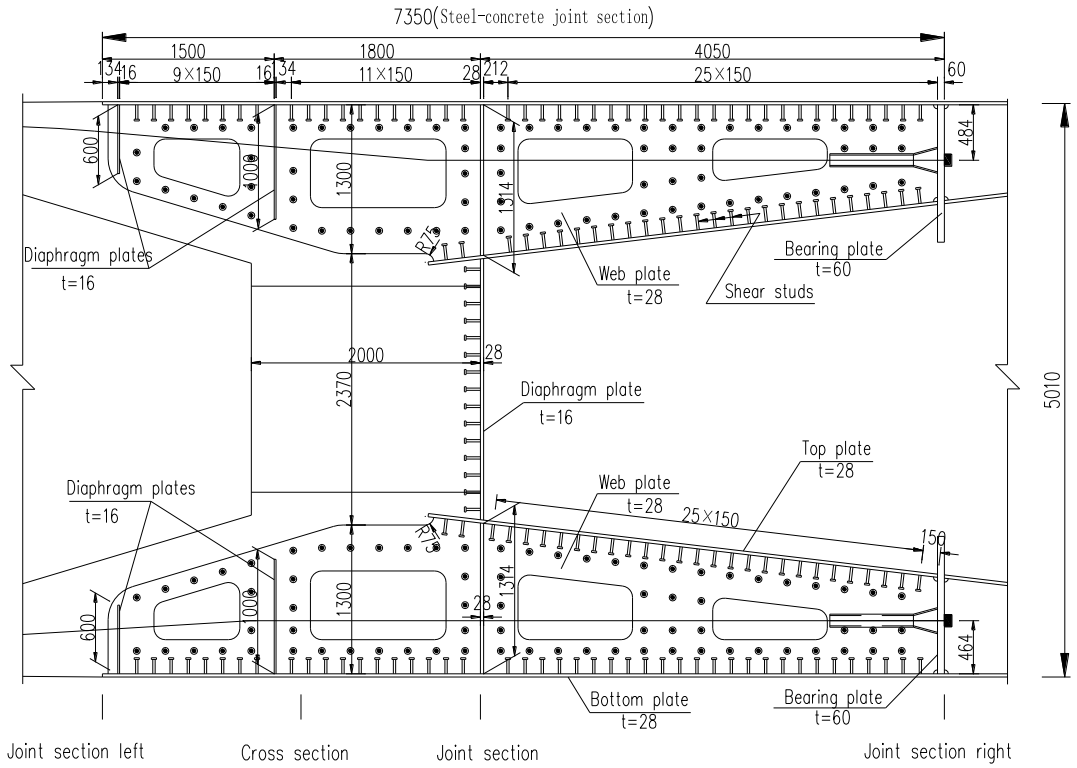

Fig. 2 Elevation view of the steel-concrete joint section in the Yong-Jiang Bridge (unit: mm)

2. Methodology

2.1. Calculation of full-bridge model

First, a full-bridge finite element model is established for the Yong-Jiang Bridge by the finite element software MIDAS/Civil (Fig. 3). Time-history curves of the internal force for positions of interest are obtained by loading a standard fatigue vehicle, thereby determining the fatigue load amplitude and cycle. For complex structures, it is difficult to ensure that the stress state of each structural member is consistent with that of the original bridge in an experimental model study, and thus, the representative weak positions are mainly ensured for equivalent stresses. In a steel-concrete joint section, the joint surface has a weaker position with greater stress, which is where problems are more likely to occur. Thus, it serves as the focus of this test. At present, there are no unified fatigue vehicles suitable for railway bridges in China. Based on a survey of China's railway operating vehicles, the train stock composed of (1DF4 +14 C64), that is, (6 × 230 + 14 × 4 × 230) kN or 14,260 kN, is used as the load for the train with the layout shown (Fig. 4). Through the finite element method for the full bridge model, the time-history curve of the internal force on the joint surface is obtained. Since the shear force has much less effect on the structure than the bending moment and axial force, its influence on the structural stress is ignored. Time-history curves of the joint surface for the axial force and the bending moment are also shown (Figs. 5-6). The calculated results suggest that the maximum and minimum stresses of the joint section occur under maximum positive and negative bending moments, respectively, which is when the fatigue stress amplitude of the joint section is largest. Using the rainflow cycle method, the internal force amplitude and the corresponding load cycles for the axial force and the bending moment of the joint surface are calculated. Meanwhile, by considering the dynamic effect and the double-line effect of a train passing a bridge, the internal force amplitude values will multiply by the impact coefficient of 1.05 and the double-line coefficient of 1.47. Each time the train passes the bridge, the internal force amplitude and the load cycles are counted as shown (Table 1), in which the impact effect and the double-line effect have already been considered in the values.

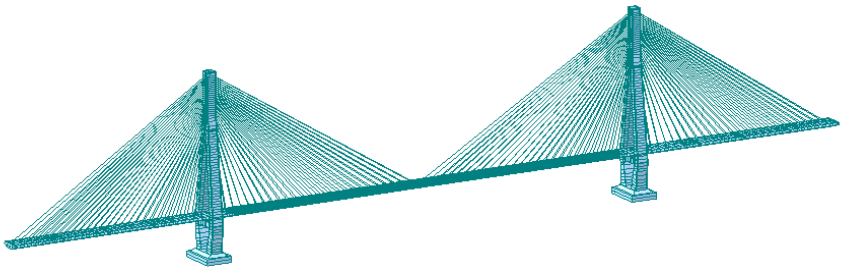

Fig. 3 Finite element model of the full-bridge bar system

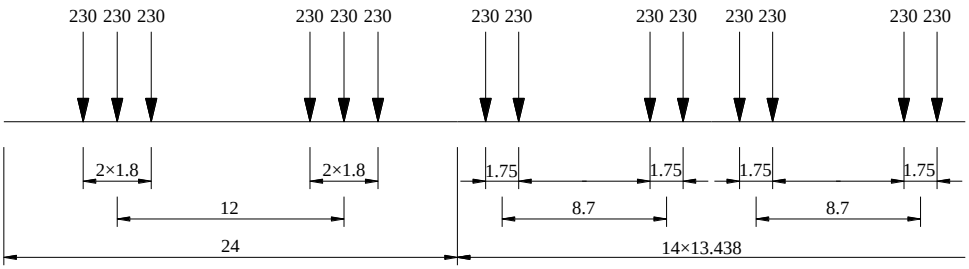

Fig. 4 Diagram of fatigue loading vehicle (unit of size: m; unit of load: kN)

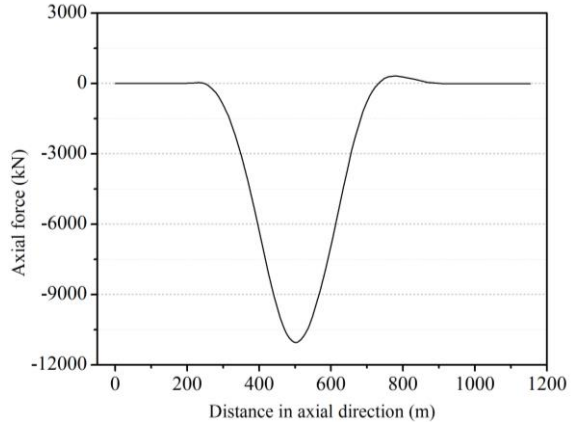

Fig. 5 Time-history curve of the axial force on the steel-concrete joint surface

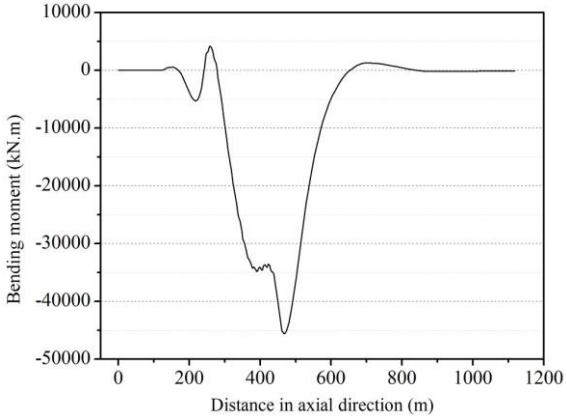

Fig. 6 Time-history curve of the bending moment on the steel-concrete joint surface

Table 1
Load spectra of the axial force and bending moment on the steel-concrete joint section

Type	Amplitude	Corresponding cycles/times
Axial force/kN	17,229.2	1
Bending moment/kN•m	74,646.48	1
	8,777.219	1
	1,879.366	1
	2,105.928	1

2.2. Test model

With such a tremendous structure and internal force transfer, it is very difficult to carry out a full-scale total cross-section model test on this steel-concrete joint section. Therefore, a bottom cell with the largest stress amplitude under a live load is selected for the full-scale model fatigue test (Fig. 1), which is based on the stress equivalence principle at the selected positions.

According to Miner's rule for cumulative linear damage caused by fatigue, the verification test after loading the fatigue model is mainly to ensure that the degree of damage in the test is the same as that of the original bridge structure over its lifetime. The variable amplitude load in the original structure may be made equivalent to the corresponding constant amplitude load. Compared to the results of a static test run once before the fatigue test, the upper and lower limits of the fatigue load are made equal to the axial force and bending moment amplitudes under the maximum positive and negative bending moments.

The test model, consistent with the original bridge structure, has a total length of 8,900 mm with a steel-concrete joint section of 7,350 mm. To avoid concentrating the stress at the ends of the model, the two ends are provided with a 1 m long concrete girder segment and a 0.55 m steel girder segment. One end of the prestressed steel tendon is anchored to the bearing plate and the other is anchored to the standard concrete box girder segment. The loading diagram of the experimental model is shown (Fig. 7). The model test uses equivalent dead and live loads. The dead weight and the internal and external prestressed forces simulate the structural dead-load stress, while loading test equipment simulates the stress amplitude produced by the live load of a train. The axial loading force of the test equipment is equivalent to the original bridge's axial force under the live load, and the equipment loading height is adjusted to achieve an equivalent bending moment of the original bridge structure under the live load. Through an equivalent calculation, the model is designed so that one of its ends is fixed and the other is free. At the cantilever end, tension-compression loading is conducted with an upper fatigue loading limit of -1,597.76 kN (compression) and a lower limit of 118 kN (tension). A diagram of the model for the load test is shown (Fig. 8).

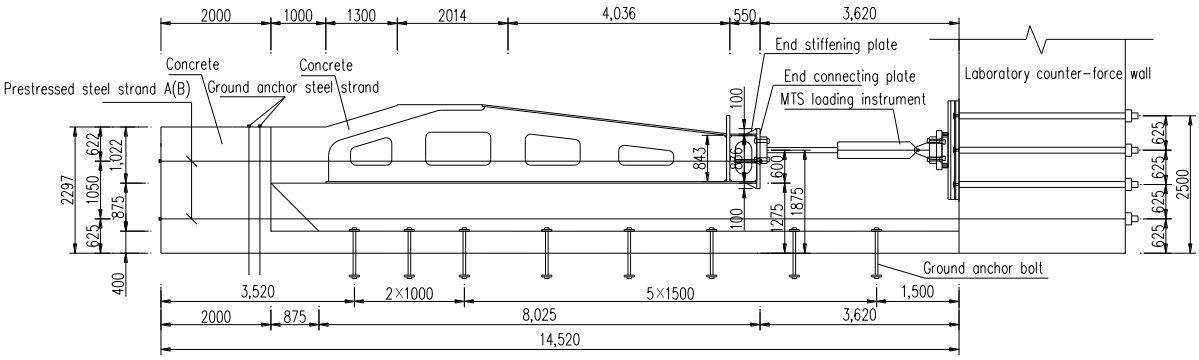

Fig. 7 Experimental model loading diagram (unit: mm)

Fig. 8 Photographs of model for load test

2.3. Determination of test load and load cycles

The Yong-Jiang Bridge is designed to have a service life of 100 years and an annual traffic volume of 27 million tons. According to the above data, within its service life, the number of fatigue loads can be calculated as follows: 2,7000,000/[(4 × 23 × 14) + (23 × 6)] × 100 = 1,893,408.

The load cycles can be calculated by Eq. (1). The number of equivalent load cycles of the axial force is 1,975,236 and that of the bending moment is 1,623,920. A fatigue verification test of 2 million load cycles will be able to achieve cumulative damage equivalence between the model and the original bridge structure under the effects of the axial force and bending moment. After the verification test is completed, the fatigue load amplitude is increased by 1.5 times for the fatigue failure test of 1 million load cycles. The whole fatigue test under loading is shown (Table 2).

$$\sum n_i \left(\Delta\sigma_i\right)^m = n\left(\Delta\sigma_0\right)^m \quad (1)$$

Table 2
Fatigue test of model under load force

Fatigue test	Load cycles/10,000 times	Load force/kN		Remarks
		Upper limit/pressure	Lower limit/tension	
Verification test	200	-1,598	118	Design load amplitude
Failure test	100	-2,400	180	1.5 times the design load amplitude

2.4. Loading equipment and test point layout

The test points of the model are mainly arranged according to the steel-concrete joint face, welding positions prone to stress concentration, and positions with high stress levels. Test points for the shear studs are mainly set at the foot of the shear studs and 30 mm away from the welding positions[24]. PBL shear connectors are composed of three members, namely, a perforated steel plate, a concrete tenon, and a penetrating reinforcing steel bar. Their static and fatigue properties are related to the performances of the three members, and the stress state of any member can reflect their mechanical performance. Therefore, test points are arranged on the penetrating steel bars of the PBL shear connectors (Figs. 9-11) to observe the mechanical performance of the group of PBL shear connectors in the steel-concrete joint section. At the free end of the model, fatigue loading is conducted using a 2,500 kN MTS hydraulic servo loading system (Fig. 12). Before fatigue loading, the model is subjected to static loading to understand the overall stress state distribution of the test model. The fatigue test is stopped for static load tests at every 20×10^4 times intervals to observe changes in the structure's static performance following cumulative damage caused by fatigue. The upper limit of the static test load is the upper limit of the structural fatigue load, which is -1,598 kN. The initial pressure applied is 0, and loading is carried out in six steps with an increase of 0.1 to 0.2 times the design load in each step.

Fig. 9 Layout of steel structure test points

Fig. 10 Layout of shear stud test points

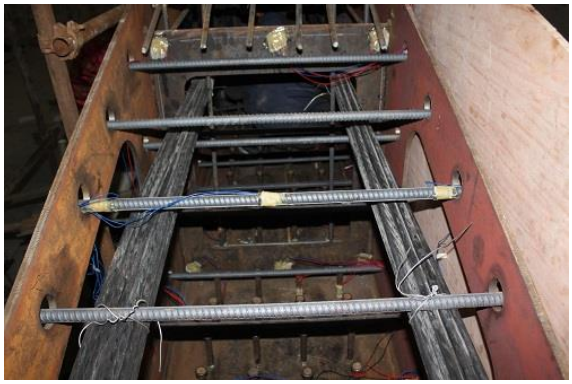

Fig. 11 Layout of PBL shear connector test points

Fig. 12 Test setup

3. Test results and analysis

3.1. Fatigue performance analysis of steel structure

According to the calculated finite element results and the measured data, it can be determined that both the stresses and stress amplitudes of the test points are relatively large at the positions where the bearing plate is welded with each plate of the steel cell. Stress-load cycle curves for the above test points are shown, where T, B, and W represent the top plate, bottom plate, and web plate, respectively (Figs. 13-15).

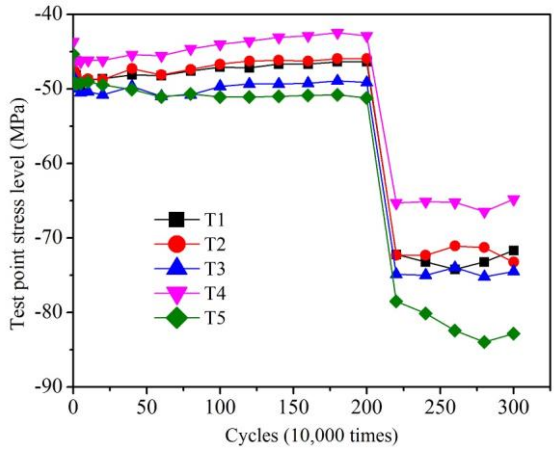

Fig. 13 Stress-load cycle curves of test points on the top plate

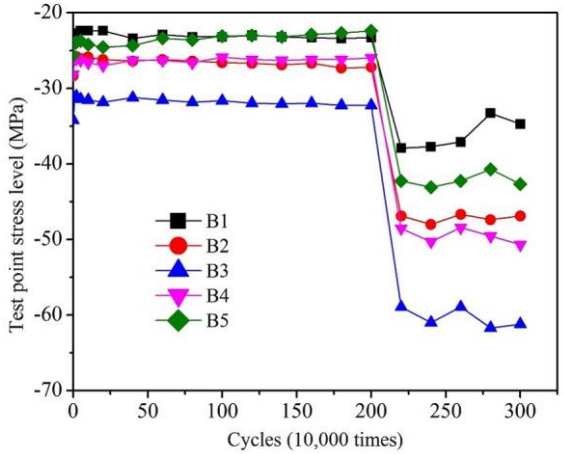

Fig. 14 Stress-load cycle curves of test points on the bottom plate

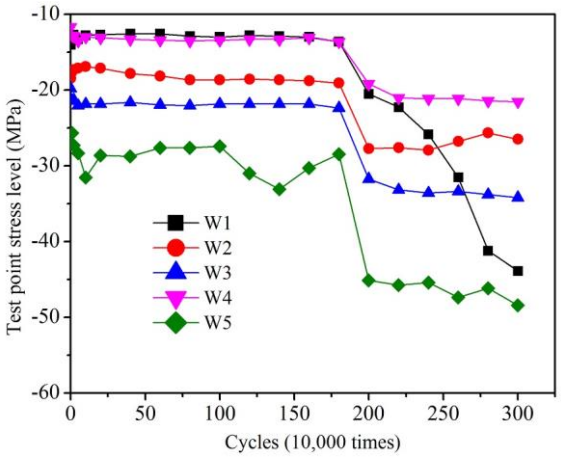

Fig. 15 Stress-load cycle curves of test points on the web plate

The stress level of the steel cell in the joint section is relatively low, and the stress value appears to be largest at the welding position on the top plate and the bearing plate (Figs. 13-15). During the fatigue verification test of 2 million cycles, the stresses of the various test points do not significantly change and fluctuate around a constant value, suggesting that the joint section has sufficient resistance against fatigue failure when the bridge is in operation. After the verification test is completed, the stress amplitude is increased by 1.5 times for the fatigue failure test of 1 million load cycles, which means that the operation time increases by 168.75 years as calculated according to Eq. (1). Load-stress curves and the variation of stress ratios of various test points are shown after the fatigue tests of 0 cycles, 400,000 cycles, 1.6 million cycles, 2 million cycles, 2.6 million cycles and 3 million cycles (Fig. 16 and Table 3). Based on the results of the fatigue failure test, all test points on the steel structure are still in an elastic state. The stress levels of the test points on the top plate experienced almost no change, and the stress levels of some test points on the bottom plate only slightly increased. Except for W1, the test points on the web plate also appear to have experienced no change in their stress levels. Located near the three welding seams between the top plate, web plate and bearing plate, the W1 test point has a complex stress condition; however, its stress is still relatively low upon completion of the fatigue failure test, satisfying relevant requirements. The longitudinal stress values for the test points on the top and bottom plates in different test phases are also shown (Figs. 17-18). The test results show that the fatigue verification test of 2 million load cycles has little effect on the force transmission performance of the steel structure. After the fatigue failure test of 1 million load cycles is completed, the influence on the force transmission performance of the steel structure is mainly present within 1,000 mm from the bearing plate, while the impact is small for the remaining positions.

Table 3
Variation of stress ratios at various test points on steel structure after fatigue test

	Fatigue stress range	Δσ1=1716kN			Δσ2=1.5×Δσ1=2580kN		
	Cycles/10,000 times	0	40	160	200	260	300
B3	Stress/MPa	-31.21	-31.21	-31.93	-50.26	-58.92	-61.18
	Stress ratio	1.00	1.00	1.02	1.61	1.89	1.96
T5	Stress/MPa	-49.23	-50.06	-50.88	-75.60	-82.40	-82.81
	Stress ratio	1.00	1.02	1.03	1.54	1.67	1.68
W1	Stress/MPa	-13.29	-12.57	-12.98	-22.25	-31.52	-43.88
	Stress ratio	1.00	0.95	0.98	1.67	2.37	3.30

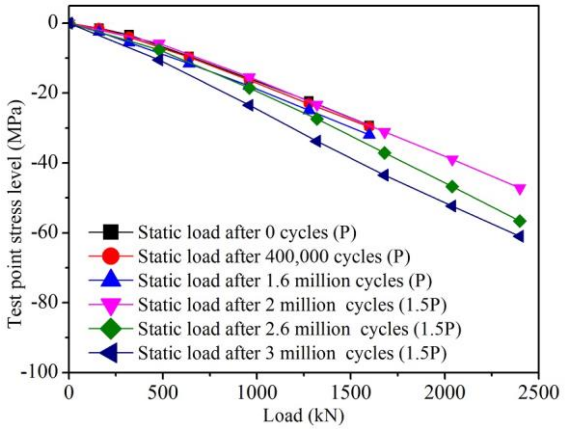

(a) Stress-load curves of the test point (B3)

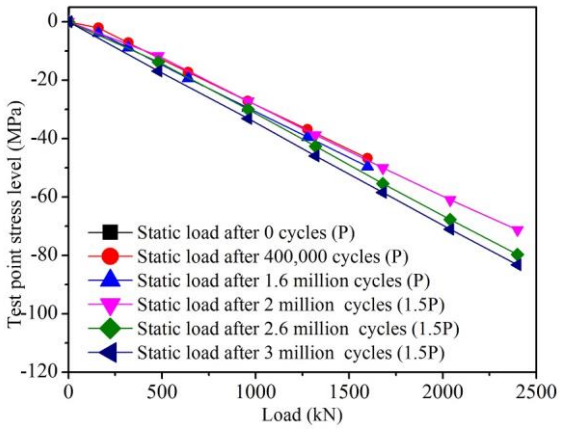

(b) Stress-load curves of the test point (T5)

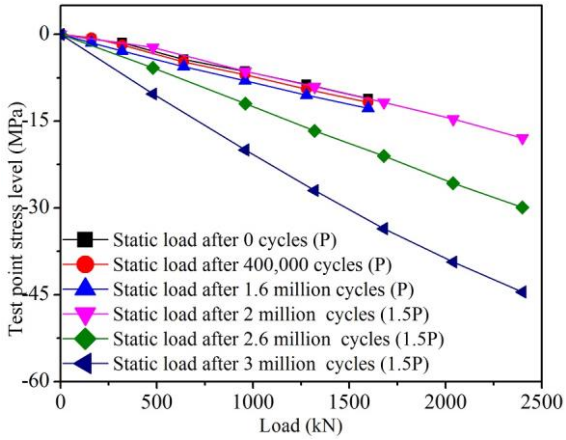

(c) Stress-load curves of the test point (W1)

Fig. 16 Load-stress curves at various test points on the steel structure after the fatigue test

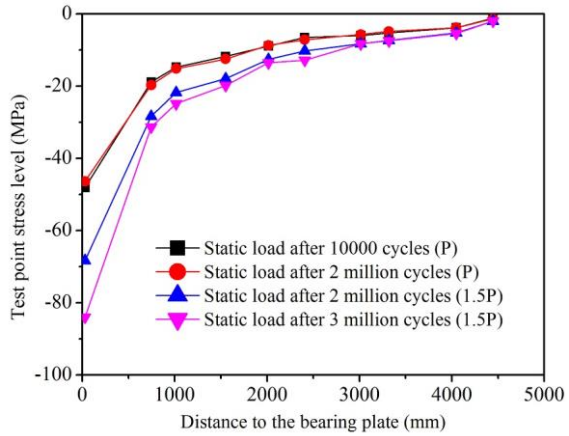

Fig. 17 Longitudinal stress values of test points on the top plate in different test phases

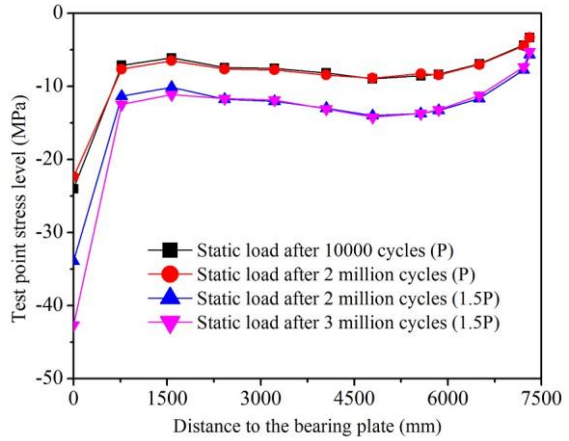

Fig. 18 Longitudinal stress values of test points on the bottom plate in different test phases

3.2. Fatigue performance analysis of shear connectors

Shear connectors serve as the main member for the transfer of the various internal forces in the steel-concrete joint section, the design rationality of which directly affects the safety performance of the whole bridge structure. Both shear studs and PBL shear connectors are used for internal force transfer in the steel-concrete joint section of the Yong-Jiang Bridge. The static load test results indicate that the PBL shear connectors and shear studs nearest the loading end experience the bulk of the stresses due to the group stud effect, and thus, the shear studs at the end near the loading end are more prone to fatigue failure. As long as the front rows of the shear studs perform well, it can be determined that the middle rows will be safe. Stress-load cycle curves of the shear connectors with greater stresses near the loading end are given, where TS and BS represent the shear studs on the top plate and bottom plate, respectively (Fig. 19). Based on the results, the stresses of the various test points on the shear connector remain basically unchanged during the fatigue verification test (0 to 2 million cycles). Load-stress curves and the variation of stress ratios of various test points are shown after the fatigue tests of 0 cycles, 400,000 cycles, 1.6 million cycles, 2 million cycles, 2.6 million cycles and 3 million cycles (Fig. 20 and Table 4). The results show that the stresses at the test points on the shear studs are in an elastic-plastic state after the fatigue test of 3 million load cycles, while those at the PBL shear connector test points have been constantly increasing but are still in an elastic state. This suggests that the load transfer in the shear studs and the PBL shear connectors is redistributed, with the load carrying ratio of the former falling and that of the latter rising, thus demonstrating good anti-fatigue performance. The stress values of various rows of shear studs on the bottom and top plates in different test phases are shown (Fig. 21). Based on these values, the fatigue load appears to have a relatively strong influence on the stresses of the shear studs near the loading end but little influence on the distant shear studs, which have a relatively low stress level. When used together, the shear studs and the PBL shear connectors work very well with each other, and the latter's high anti-fatigue performance is fully demonstrated under fatigue loads. With continuous fatigue loads, the shear studs at the end decrease overall in stiffness, and the PBL shear connectors increase in shear force.

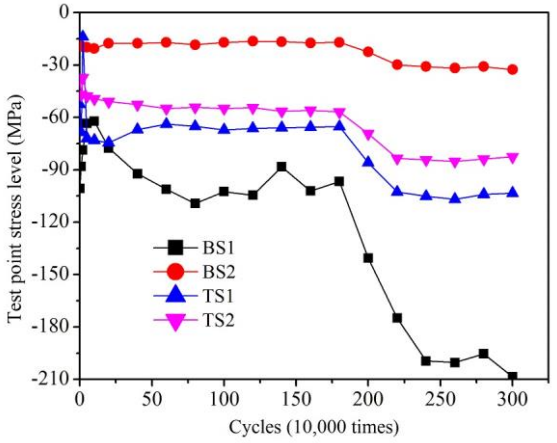

(a) Stress-load cycle curves of test points on shear studs

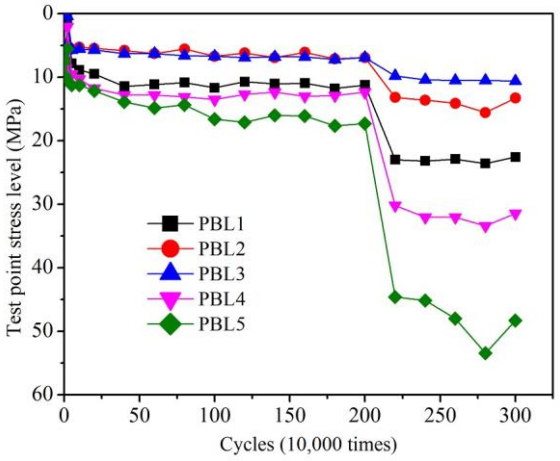

(b) Stress-load cycle curves of test points on PBL shear connectors

Fig. 19 Stress-load cycle curves of test points on main shear connectors

Table 4
Variation in stress ratios at various test points on shear connector tests after fatigue testing

	Fatigue stress range	Δσ1=1716kN			Δσ2=1.5×Δσ1=2580kN		
	Cycles/10,000 times	0	40	160	200	260	300
BS1	Stress/MPa	93.52	96.00	106.09	147.70	204.56	212.39
	Stress ratio	1.00	1.03	1.13	1.58	2.19	2.27
TS2	Stress/MPa	-31.72	-32.14	-34.20	-78.90	-34.61	-29.05
	Stress ratio	1.00	1.01	1.08	2.49	1.09	0.92
PBL5	Stress/MPa	10.92	12.98	16.27	24.10	48.00	46.35
	Stress ratio	1.00	1.19	1.49	2.21	4.40	4.25

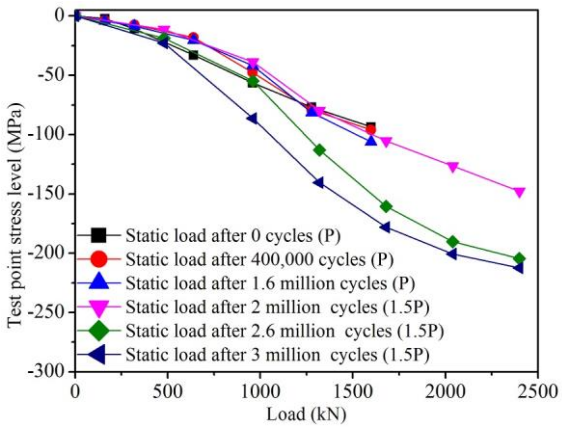

(a) Stress-load curves of the test point (BS1)

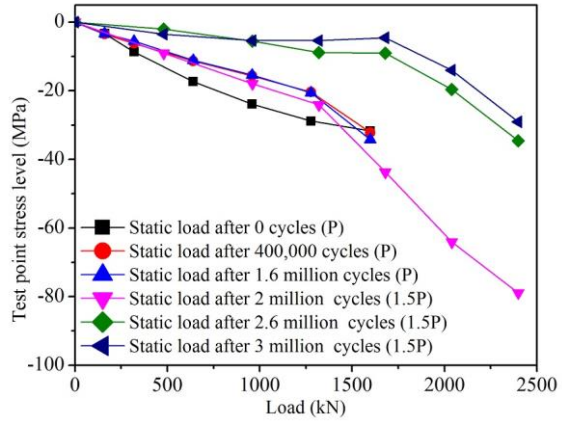

(b) Stress-load curves of the test point (TS2)

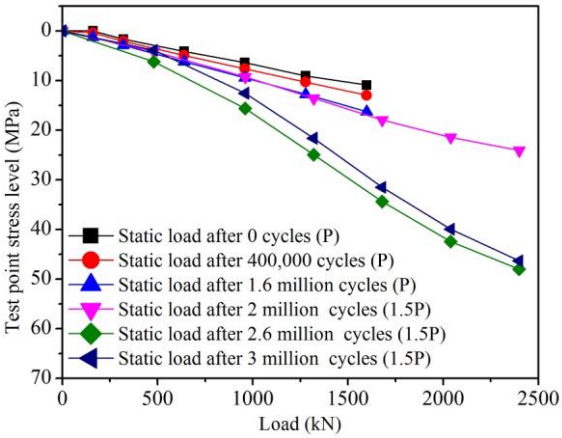

(c) Stress-load curves of the test point (PBL5)

Fig. 20 Load-stress curves at various test points on shear connectors after fatigue testing

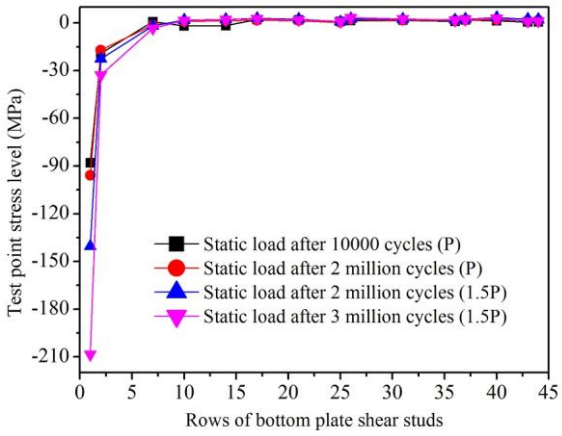

(a) Shear studs on the bottom plate

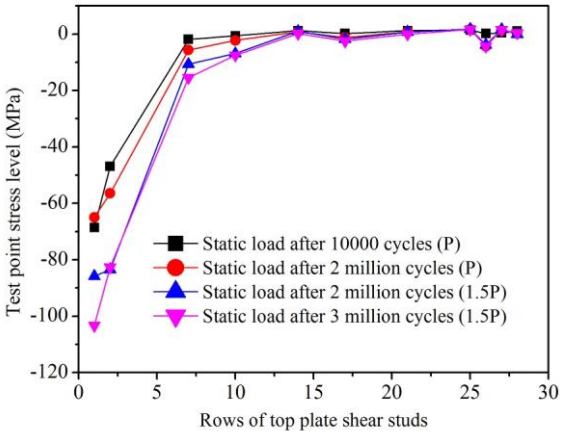

(b) Shear studs on the top plate

Fig. 21 Stress values of test points on various rows of shear studs in different test phases

3.3. Fatigue performance analysis of concrete girder

Stress-load cycle curves for the concrete test points are shown (Fig. 22). The stress ratios of various test points are shown after the fatigue tests of 0 cycles, 400,000 cycles, 1.6 million cycles, 2 million cycles, 2.6 million cycles and 3 million cycles (Table 5). The results show that the stress level of the concrete girder is low in the fatigue verification test (0 to 2 million cycles), and the stresses of the various test points fluctuate within a certain range. After the fatigue test of 3 million cycles is completed, the stress level of the concrete structure remains basically unchanged, indicating that the effect of the fatigue load on the concrete structure is very small.

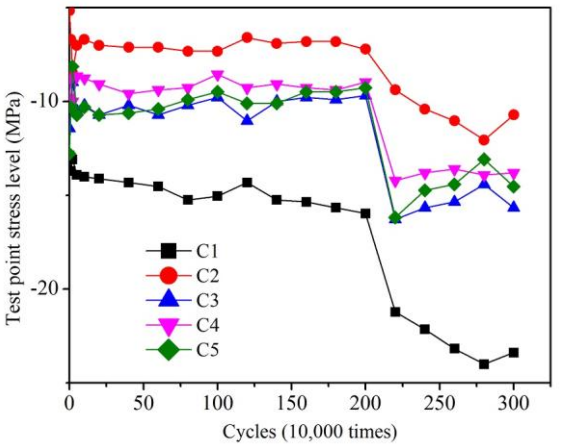

Fig. 22 Stress-load cycle curves of the main test points on the concrete girder

Table 5
Variation in stress ratios at various test points on concrete girder tests after fatigue testing

	Fatigue stress range	Δσ1=1716kN			Δσ2=1.5×Δσ1=2580kN		
	Cycles/10,000 times	0	40	160	200	260	300
C1	Stress/MPa	-13.70	-14.32	-15.35	-20.29	-23.18	-23.38
	Stress ratio	1.00	1.05	1.12	1.48	1.69	1.71
C3	Stress/MPa	-10.20	-10.20	-9.79	-15.35	-15.35	-15.66
	Stress ratio	1.00	1.00	0.96	1.51	1.51	1.54

4. Conclusions

The fatigue performance of the steel-concrete joint section of a railway hybrid girder cable-stayed bridge was analysed using a model test in this paper. The following conclusions were drawn:

(1) The stress at various test points in the steel structure of the steel-concrete joint section exhibits little change during the fatigue verification test of 2 million load cycles. However, only the stress of the test points on the bottom plate slightly increases after the fatigue test of 3 million load cycles.

After the fatigue test of 3 million load cycles, the stress levels of the concrete test points exhibit no change. The stress of the steel structure and concrete structure of the joint section is still low after all fatigue tests, indicating that the steel structure and concrete structure essentially experience no damage caused by fatigue.

(2) The stress of the test points on the shear connectors slightly changes after the fatigue verification test of 2 million load cycles. Between 2 million and 3 million fatigue load cycles, the stress values of the PBL shear connectors gradually increase. The shear studs with larger stresses near the loading end enter an elastic-plastic state, and the overall rigidity decreases after all fatigue tests. The shear force transfer in the shear studs and the PBL shear connectors is redistributed, with the load carrying ratio of the former falling and that of the latter rising. The two kinds of shear connectors work well with each other.

(3) Following the test, the model is checked. Overall, the structural performance is good and does not exhibit localized damage or instability. In addition, the joint section shows no slip failure or exterior cracks, and the concrete structure has no scaling. The above results indicate that the design of the joint section is reasonable with good anti-fatigue performance.

References

[1] Xiang H.F., “Major technical innovations in world’s bridge development”, Guangxi Communication Science and Technology, 28(5), 1-7, 2003.

[2] Nie, J.G., Tao, M.X., Wu, L.L., Nie X. and Li F.X., “New progress in the study of steel-concrete composite bridge”, China Civil Engineering Journal, 45(06), 110-122, 2012.

[3] Jaspart J.P. and Weynand K., “Design of joints in steel and composite structures. ECCS Eurocode Design Manuals”, ECCS - European Convention for Constructional Steelwork, 2016.

[4] Liang X., Duan S.J., Wang Y.Y. and Zhang Y.Q., “Experimental and theoretical study on the behavior of the laminated action of steel-concrete composite beam in negative bending moment region”, Advanced Steel Construction, 16(3), 216-222, 2020.

[5] Liu Y.Q., “Steel-concrete hybrid bridge”, Beijing: China Communications Press, 2005.

[6] Bouazaoui L., Perrenot G., Delmas Y. and Li A., “Experimental Study of bonded Steel Concrete composite structure”. Journal of Constructional Steel Research,63(9), 1268-1278, 2007.

[7] Evangelos J. S. and John T.K., “ Interface forces in composite steel-concrete structure”, International Journal of Solids and structures, 37(32), 4455-4472, 2000.

[8] He J., Liu Y.Q. and Pei B.Z., “Experimental Study of the Steel-Concrete Connection in Hybrid Cable-Stayed Bridges”, Journal of Performance of Constructed Facilities, 28(3),559-570, 2014.

[9] Wei X. and Qiang S.Z, “Specimen test for mechanics behavior of steel-concrete composite joint in pylon of cable-stayed bridge”, Engineering Mechanical, 30(1), 255-260, 2013.

[10] Zhang Z.X., Huang C.P. and Xu H.Y., “Force transfer mechanism for steel-concrete composite structures of hybrid cable-stayed bridges”, Journal of Huazhong University of Science and Technology(Natural Science Edition), 38(5), 117-120, 2010.

[11] Dai X.X., Liew J.Y.R. “Fatigue performance of lightweight steel-concrete-steel sandwich systems”, Journal of Constructional Steel Research, 66(2), 256-276, 2010.

[12] Lee P.G., Shim C.S.and Chang S.P., “Static and fatigue behavior of large stud shear connectors for steel–concrete composite bridges”, Journal of Constructional Steel Research, 61(9), 1270-1285, 2005.

[13] Lowes L.N. and Arash A., “Modeling reinforced-concrete beam-column joints subjected to cyclic loading”, Journal of Structural Engineering, 129(12),1686-1697, 2003.

[14] Wei X., Xiao L., Shao K.F. and Jiang S., “Fatigue performance of perfobond shear connector in steel-concrete composite structure”, China Journal of Highway and Transport, 43(4), 80-86, 2013.

[15] Zhou Y.T., Bao W,G., Zhai H. and Liu Y.F., “Study of standard fatigue design load for steel highway bridges”, China Civil Engineering Journal ,43(11), 79-85. 2010.

[16] Pan J.Y., “Design on fatigue reliability of railway steel bridge and study on fatigue load spectrum of railway bridge”, Journal of the China Railway Society, 14(4), 58-66, 1992.

[17] Li Y.D. and Xu J., “Analysis of Fatigue Damage Probability for Steel Railway Bridges”, Bridge Construction, 33(4), 1-10, 2003.

[18] Hanswille G., Porsch M. and Ustundag C., “Resistance of headed studs subjected to fatigue loading Part II: Analytical study”, Journal of Constructional Steel Research, 63(4), 485-493, 2007.

[19] Jeong Y.J., Kim S.H. and Ahn J.H., “Partial-interactive behavior of steel–concrete member under static and fatigue loadings”, Magazine of Concrete Research, 57(5), 289-300, 2005.

[20] Jeong Y.J., Kim H.Y. and Kim S.H., “Partial-interaction analysis with push-out tests”, Journal of Constructional Steel Research, 61(9), 1318-1331, 2005.

[21] Kim S.H., Lee C.G., Kim S.J. and Won J.H., “Experimental study on joint of spliced steel-PSC hybrid girder, part II: Full-scale test of spliced hybrid I-girder”, Engineering Structures, 33(9), 2668-2682, 2011.

[22] Jie Z.Y., Li Y.D., Wei X. and Zhuge P., “Fatigue life assessment of inclined welded joints in steel bridges subjected to combined normal and shear stresses”, Advanced Steel Construction, 14(4), 620-633, 2018.

[23] Jie Z.Y., Wu J.W., Zhuge P., Li Y.D. and Wei X., “Fatigue properties of inclined cruciform welded joints with artificial pits”, Advanced Steel Construction, 17(1), 20-27, 2021.

[24] Cui C., Zhang Q.H., Bao Y., Bu Y.Z. and Luo Y., “Fatigue life evaluation of welded joints in steel bridge considering residual stress”, Journal of Constructional Steel Research, 153(2), 509-518, 2019.